Biomaterials Science

PAPER

Cite this: *Biomater. Sci.*, 2018, **6**, 2230

Self-assembled phosphate-polyamine networks as biocompatible supramolecular platforms to modulate cell adhesion†

Nicolás E. Muzzio, [a] Miguel A. Pasquale, [a] Waldemar A. Marmisollé,[a] Catalina von Bilderling, [a,c] M. Lorena Cortez, [a] Lía I. Pietrasanta[b,c] and Omar Azzaroni *[a]

The modulation of cell adhesion *via* biologically inspired materials plays a key role in the development of realistic platforms to envisage not only mechanistic descriptions of many physiological and pathological processes but also new biointerfacial designs compatible with the requirements of biomedical devices. In this work, we show that the cell adhesion and proliferation of three different cell lines can be easily manipulated by using a novel biologically inspired supramolecular coating generated *via* dip coating of the working substrates in an aqueous solution of polyallylamine in the presence of phosphate anions—a simple one-step modification procedure. Our results reveal that selective cell adhesion can be controlled by varying the deposition time of the coating. Cell proliferation experiments showed a cell type-dependent quasi-exponential growth demonstrating the nontoxic properties of the supramolecular platform. After reaching a certain surface coverage, the supramolecular films based on phosphate–polyamine networks displayed antiadhesive activity towards cells, irrespective of the cell type. However and most interestingly, these antiadherent substrates developed strong adhesive properties after thermal annealing at 37 °C for 3 days. These results were interpreted based on the changes in the coating hydrophilicity, topography and stiffness, with the latter being assessed by atomic force microscopy imaging and indentation experiments. The reported approach is simple, robust and flexible, and would offer opportunities for the development of tunable, biocompatible interfacial architectures to control cell attachment for various biomedical applications.

Received 6th March 2018,
Accepted 28th June 2018

DOI: 10.1039/c8bm00265g

rsc.li/biomaterials-science

1. Introduction

One of the major goals in tissue engineering and regenerative medicine is the development of novel materials and surface coatings[1–3] with controllable mechanical and biological characteristics that enhance cell adhesion and modulate long-term tissue cell behavior,[4] establishing complex interactions to develop proper biocompatibility pathways.[5]

Cells must adhere well to fabricated scaffolds or to the surface of implants, prior to any complex mechanism taking place in tissue regeneration. For good cell adhesion and spreading it is necessary that the substrate stiffness be adequate to generate forces to balance the intracellular tension generated by stress fibers.[6] As a cell adheres to a substrate or matrix and actively senses the local elastic resistance of the matrix and nearby cells *via* their deformation and feedback, recognition mechanisms seem to be triggered.[7] Furthermore, matrix stiffness and topography regulate normal and neoplastic cell mechanics and motility[8] and may determine cancer cell malignancy through a complex mechanism.[9]

Selective adhesion has been achieved between endothelial and muscle cells by changing the mechanical properties of substrates by coating with different polymeric thin films.[10] In this case, stiffness modulation was based on the fact that cells can sense the stiffness of objects that are not in direct contact, similarly to "the princess who feels a pea placed below her mattress",[11] depending on the polymer coating thickness as well as on its chemical and physical properties.

It is desirable for any material with potential biomedical applications to be based on biocompatible elements that do

[a]*Instituto de Investigaciones Fisicoquímicas Teóricas y Aplicadas (INIFTA), (UNLP, CONICET), Sucursal 4, Casilla de Correo 16, 1900 La Plata, Argentina. E-mail: azzaroni@inifta.unlp.edu.ar; http://softmatter.quimica.unlp.edu.ar*
[b]*Instituto de Física de Buenos Aires (IFIBA, UBA-CONICET), and Centro de Microscopías Avanzadas, Facultad de Ciencias Exactas y Naturales, Universidad de Buenos Aires, C1428EHA Buenos Aires, Argentina*
[c]*Departamento de Física, Facultad de Ciencias Exactas y Naturales, Universidad de Buenos Aires, C1428EHA Buenos Aires, Argentina*

†Electronic supplementary information (ESI) available. See DOI: 10.1039/c8bm00265g

not have a negative impact on proliferation. Furthermore, the material should be capable of adsorbing a certain amount of proteins from the cell media, as cells adhered to a substrate do not interact directly with the material surface but with the proteins coming from biological fluids deposited thereon.[12,13]

A large number of different materials mimicking the interactions between cells and their environment have been employed, namely, natural and synthetic polyelectrolyte multilayers (PEMs), protein-coated polyacrylamide or poly(dimethylsiloxane) polymeric substrates with tunable stiffness,[14] hydrogels that can be biochemically and mechanically altered by chemical functionalization or by changing hydrogel cross-linking density, respectively.[15] Furthermore, microgels have been used alone to fabricate thin film substrates or as constitutive units combined with other polyelectrolytes.[16] For practical *in vivo* applications, particularly long-time ones, the approval of any of the reagents employed in the synthesis due to their possible toxicity is a comprehensible limitation.

On the other hand, bio-inspired supramolecular chemistry is a fascinating strategy to build up highly functional systems from relatively simple molecules based on non-covalent interactions.[17–19] Surface chemistry concepts can enrich the perspective of supramolecular chemistry applications. A well-known example is the use of a mussel-inspired biomimetic surface coating obtained by the spontaneous self-polymerization of dopamine leading to the formation of thin, surface-adherent polydopamine films onto a wide variety of substrates. This methodology introduces a novel material-independent strategy to modify the material surface properties[20–23] and to develop free-standing hydrogel with potential biomedical applications.[24] More recently, motivated by the large number of applications of polydopamine in surface science, other biologically inspired phosphate/polyamine-based thin multifunctional films have been proposed.[25] In this case, the self-organization of polyamine and phosphate ions is driven by non-covalent interactions as occurs in numerous biological systems. For instance, nuclear aggregates of polyamines (NAPs) are present in many cells to efficiently protect and modulate the DNA in cell nuclei.[26] Although electrostatic interactions appeared to be the prevailing interactions, hydrogen bonds are also thought to play a key role in stabilizing the spatial structure of NAPs.[27]

Nature has developed elegant self-assembly-based synthetic routes to produce biosilica involving polyamines and silaffins.[28] For instance, in diatom photosynthetic algae[29] a variety of highly ordered mineral structures are produced. Diatoms also contain inorganic phosphate, and it appears that microscopic phase separation is driven by polyamines and highly phosphorylated silaffin aggregation is induced by phosphate ions.[30,31]

Poly(allylamine hydrochloride) (PAH) has been extensively employed as a polyamine model and through the interaction with multivalent anions such as phosphate or sulfate efficiently induces a microscopic phase separation.[32] This process is driven in the 4–9 pH range, where charged species undergo electrostatic interactions, and the formation of a hydrogen bond network is responsible for the particle aggregation required for microscopic phase separation.[30] Orthophosphate anions meet the structural geometric requirements and have the ability to form hydrogen bonds. Pyrophosphate and tripolyphosphate anions are also able to efficiently induce PAH aggregation and when their concentration is high enough, they produce a macroscopic gelled precipitate that adheres to both hydrophilic and hydrophobic surfaces.[33,34] In general, supramolecular chemistry is built by very large macromolecules that may be of natural or synthetic origin, but the final properties and behavior, particularly in relation to biological interfaces, are greatly regulated by the content and structure of water.[35,36]

In this work we apply this novel biomimetic phosphate/polyamine-based platform to modulate cell adhesion properties and proliferation on both adherent and nonadherent substrates. Two simple strategies were adopted: the Pi/PAH coating thickness was controlled by varying the deposition time (t_D), and thermal annealing of dried coated samples was performed. Thus, employing a simple procedure based on a one-pot supramolecular assembly, we are able to: (i) induce cell adhesion on nonadherent substrates at short deposition times (<40 min); (ii) promote an antiadhesive behavior on adherent substrates for longer modification times (>120 min); (iii) restore or enhance the cell adhesion by thermal annealing of dried Pi/PAH-coated samples. These goals are summarized in Scheme 1. Three different cell lines, consisting of an epithelial cell line from cervix carcinoma (HeLa cells), murine myoblast (C2C12 cells) and murine preosteoblast (MC3T3 cells), were utilized. Experimental data confirmed the biocompatibility of the proposed novel material for the culture time tested and suggest that cell-sensed stiffness plays a key role in cell adhesion, exhibiting a cell-dependent behavior. On the other hand, the thermal annealing of the coating induces the film reorganization and generates a cell-sensed stiffer surface that improves cell adhesion properties in comparison to native Pi/PAH substrates.

2. Experimental

2.1. Materials and reagents

Poly(allylamine hydrochloride), 58 kDa, sodium chloride, 4-(2-hydroxyethyl)piperazine-1-ethanesulfonic acid sodium salt (HEPES), phosphate-buffered saline (PBS, D1408), sodium dodecyl sulfate (SDS, L6026), Triton X-100 (T8787), Tween-20 (P9416) and fibronectin (FN) from bovine plasma (F4759) were purchased from Sigma-Aldrich. KH_2PO_4 (Pi) was supplied by Biopack (Argentina), RPMI 1640 with L-glutamine was purchased from Fisher, minimum essential medium (MEM) was acquired from Sigma-Aldrich and fetal bovine serum (FBS) from Natacor (Argentina). The reagent MTT (3-(4,5-dimethylthiazol-2-yl)-2,5-diphenyltetrazolium bromide) was provided by Thermo Fisher Scientific, and dimethyl sulfoxide by Biopack

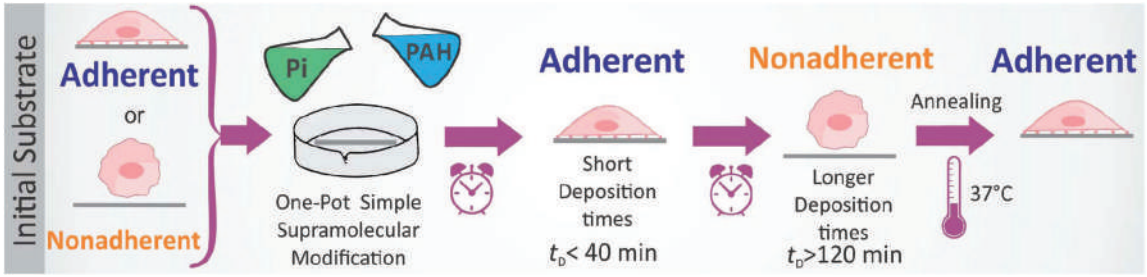

Scheme 1 Procedure and modification steps to modulate the cell adhesion on both initially adherent and nonadherent substrates by deposition of the supramolecular self-assembled coating of polyamine (PAH) and phosphate (Pi).

(Argentina). Deionized water was obtained using the Milli-Q water purification system.

2.2. Pi/PAH-coated substrate preparation

Pi/PAH-coated substrates were fabricated from stock solutions of PAH (1 mg mL^{-1}) and Pi (10 mM KH_2PO_4) both at pH = 7. Polystyrene or glass substrates of appropriate size were cleaned by immersion in 10 mM sodium dodecyl sulfate (SDS) from Sigma-Aldrich for 3 h and rinsed three times in deionized water. PAH and Pi solutions were mixed at a final concentration of 0.05 mg mL^{-1} and 5 mM, respectively, in a beaker with the cleaned substrates at the bottom and left for the desired deposition time (t_D). After deposition of the coating, samples were rinsed with deionized water. Coating thickness was measured in samples with different t_D. For this purpose a thin linear furrow was scraped in samples employing a small needle, and the depth of the furrow was assessed by atomic force microscopy (AFM). Measurements were performed in air died samples, and results were plotted as thickness *versus* t_D (Fig. S1 in the ESI†).

2.3. Annealing of Pi/PAH-coated substrates

Films prepared as described in the previous section were dried and left in the cell culture incubator at 37 °C in 5% CO_2 and at 97% humidity for 3 days (thermal annealing). This treatment was employed following previous investigations that indicate the improvement in the adhesion of several cell lines to poly-L-lysine/alginic acid films after treatment at the above-mentioned conditions.[37] As in our previous work, in this case we observed that no effect on film properties and concomitantly on cell adhesion characteristics was observed for the thermal treatment of samples immersed in phosphate buffer solution (PBS) or dried and left for 3 days at ambient temperature.

2.4. Atomic force microscopy

AFM measurements were performed in aqueous solution (10/150 mM HEPES/NaCl buffer, pH = 7.4, "HEPES buffer") using a Multimode 8 AFM (Nanoscope V Controller, Bruker, Santa Barbara, CA). V-shaped SNML AFM probes (Bruker, 0.07 N m^{-1} cantilever nominal spring constant) were used.

Images were acquired either in tapping mode (TM, Bruker) or in peak force tapping mode (PeakForce-Quantitative NanoMechanics, QNM, Bruker). QNM was performed at 0.25 kHz. Topography images and rms roughness were analyzed using the commercial Nanoscope Analysis software (Bruker). Force curve analysis was performed using custom-made Matlab routines (Mathworks).

For each experimental condition, the exact spring constant of the cantilever was determined using the thermal tune method,[38] and the deflection sensitivity was calibrated in fluid using a freshly cleaved mica sample as an infinitely stiff reference material.

Individual force–distance curves (FDC) were selected at specific sample locations from the QNM maps. The contact point of each FDC was determined according to a published algorithm.[39] Stiffness was obtained by the Sneddon's contact mechanics model, assuming a parabolic tip and a plane surface contact. Knowledge of the force applied to the indenter as a function of the penetration during the loading experiment allows for the calculation of the Young's modulus E using a numerical form of the Sneddon's equation for AFM data:[40,41]

$$E_i = \frac{1}{2\sqrt{R}\beta}(1-\nu)k\frac{\Delta z_{\mathrm{def}\ i,i-1}}{\sqrt{h}\Delta h_{i,i-1}} \quad (1)$$

where R is the radius of curvature of the tip, β is assumed to be equal to 2 for elastic spherical deformation, and k is the cantilever vertical spring constant. The Poisson's ratio ν was assumed to be 0.5. The indentation depth $h = z_{\mathrm{pos}} - z_{\mathrm{def}}$, z_{def} being the measured vertical deflection of the cantilever, and z_{pos} the vertical displacement of the piezoelement; i, $i-1$ refers to adjacent tip displacements.

Eqn (1) allows the calculation of the elastic modulus E_i as a function of the penetration. The elastic modulus for the examined samples was relatively independent of indentation depth at indentation depths larger than 5 nm. Below this depth value, unstable results, commonly related to the destabilizing attractive force gradient in the vicinity of surfaces, were obtained.[40] For each FDC, the mean elastic modulus was evaluated by averaging the Young's modulus obtained for indentations above 5 nm. The obtained stiffness was not found to increase at the highest indentation values, thus it is possible to confirm that the substrate contribution was avoided in the measurements.

2.5. Contact angle and ζ-potential measurements

The wettability of Pi/PAH-coated substrates was measured on air-dried samples in a DSA 100 contact angle measuring system (Ramé Hart 200). The tangent angle of a three-phase contact point of a sessile drop profile of millipure water on the surfaces was determined. Images were analyzed employing the DROP Image Advanced 2.2v software. The volume of the droplet was kept constant (3 μL), while the velocity was set at 500 μL min^{-1}. Four repetitions were conducted for each sample.

The ζ-potential was measured on 4 mm wide and 5 mm long Pi/PAH-coated coverslips using phase analysis light scattering and modelling the electroosmotic flow near the surface of the samples.[42] For this purpose, a Zetasizer Nano ZS (Malvern Instruments Ltd, Malvern, UK) was employed. Samples were attached to a holder and then placed between two electrodes utilizing a dip cell device (ZEN1020) and quartz cell with 1 cm optical path. Latex particles (zeta potential transfer standard DTS 1235, Malvern Instruments Ltd) dispersed in 100 mM NaCl were employed as tracers. Three independent experiments were performed for each sample.

2.6. Protein adsorption from quartz crystal microbalance measurements

The quartz crystal microbalance with dissipation (QCM-D) Q-Sense E4 system was employed to test protein adsorption on unannealed and annealed Pi/PAH-coated substrates. Fibronectin (FN) was utilized as an adhesion promoting protein model. The coating of Pi/PAH polymer was conducted on SiO_2 (50 nm) coated quartz crystals (5 MHz, Q-Sense) out of the chambers and eventually annealed. Then, crystals were mounted in the chambers and first HEPES buffer was passed through the chamber, and subsequently 20 μg mL^{-1} FN solution was injected *via* a peristaltic pump. After the appropriate flowing time, rinsing with HEPES buffer was performed.

2.7. Cell culture

A HeLa epithelial cell line from a human cervix carcinoma, C2C12, a mouse myoblast cell line, and MC3T3 murine preosteoblast were incubated at 37 °C in 5% CO_2 and 97% humidified atmosphere and grown in RPMI medium in the case of the first two cell lines and in alpha-MEM for the latter cell line. Both media were supplemented with 10% FBS and antibiotics.

For adhesion assays, the Pi/PAH complex was deposited on top of circular glass slides 1.4 cm in diameter, or at the bottom of 24-well cell culture polystyrene plates (Greiner Bio-One) and UV-sterilized for 1 h. Then, 20 000 cells in 1 mL culture medium were seeded on top. Eventually, bacteriological polystyrene wells 5 cm in diameter were used as nonadherent surfaces, and 100 000 cells in 5 mL culture medium were seeded. Phase-contrast images were taken employing a Nikon T100 inverted microscope with a CFI flat field ADL 10× objective.

2.8. Quantification of cell adhesion

The cell adhesion and spreading characteristics of each cell line were quantified 1–4 days after seeding. For this purpose, cell contours were manually traced using a Wacom graphic table and analyzed using Image Pro Plus 6.0 software (Media Cybernetics Inc.). The cell area, measured in μm^2, and the aspect ratio, the ratio between the major and minor axes of an ellipse with area equivalent to that of the cell, were determined.

Differences in the average cell adhesion area and morphological parameters for each tested substrate were evaluated utilizing one-way analysis of variance (ANOVA) and Fisher test with a significance level $p = 0.05$.

Fluorescent staining of vinculin, actin and cell nucleus was performed following the protocol described in the Actin Cytoskeleton and Focal Adhesion Kit user manual (FAK100 from Millipore) to further assess details of cell adhesion characteristics. Anti-vinculin primary antibody and anti-mouse IgG-FITC conjugated antibody (secondary antibody) were used for vinculin protein staining. TRITC-conjugated phalloidin and 4′,6-diamidino-2-phenylindole (DAPI) were used for F-actin and nucleus staining, respectively. Stained cells were observed by Confocal Laser Scanning Microscope (Carl-Zeiss LSM 10 META).

2.9. MTT viability assay

For MTT experiments, samples were assembled at the bottom of 24-well polystyrene plates, or occasionally on circular coverslips (1.4 cm in diameter), and placed in 24-well polystyrene plates. Approximately 20 000 cells were seeded adding 1 mL of medium. After the appropriate times of incubation, 80 μL of MTT solution (5 mg mL^{-1} in 10 mM PBS) were added to each well. Cells were incubated in the presence of the MTT solution for 3 h at 37 °C. Then, the culture medium was completely removed, and the formazan products were solubilized by adding 600 μL of DMSO to each well. The absorbance spectra were measured at 550 nm by a plate reader (Genios Pro). Measurements were repeated three times, and the mean value and its standard deviation were reported for each condition.

3. Results and discussion

3.1. Pi/PAH modified substrates for tuning cell adhesion

The adhesion properties and viability of cervix carcinoma (HeLa cells), murine myoblast (C2C12 cells) and murine preosteoblast (MC3T3 cells) on Pi/PAH-based coatings are presented. These cell lines proceed from tissues with different properties, presenting different environmental conditions to cells, thus resulting of interest to test the proposed material. C2C12 and MC3T3 cells are commonly used to develop materials with biomedical applications. HeLa cell is a well-known cancerous cell model to study individual and collective behaviors related to cancer processes; new materials could be useful to control and model tumoral conditions.

Cell adhesion was evaluated for the control surface, glass or PS of the culture wells, and Pi/PAH films with increasing deposition time (t_D), ranging from 20 to 180 min (Fig. 1 and 2). For this range of t_D, the thickness (see Fig. S1 in the ESI†) as well as the film mass of the coating follow an increasing monotonous relation with the deposition time. From t_D = 120 min afterwards a plateau is reached for the mass,[25] and the rate of the coating thickness increase significantly decreases. For t_D values of 20, 30, 40, 60, 90, 120 and 180 min, a thickness of 25, 40, 60,

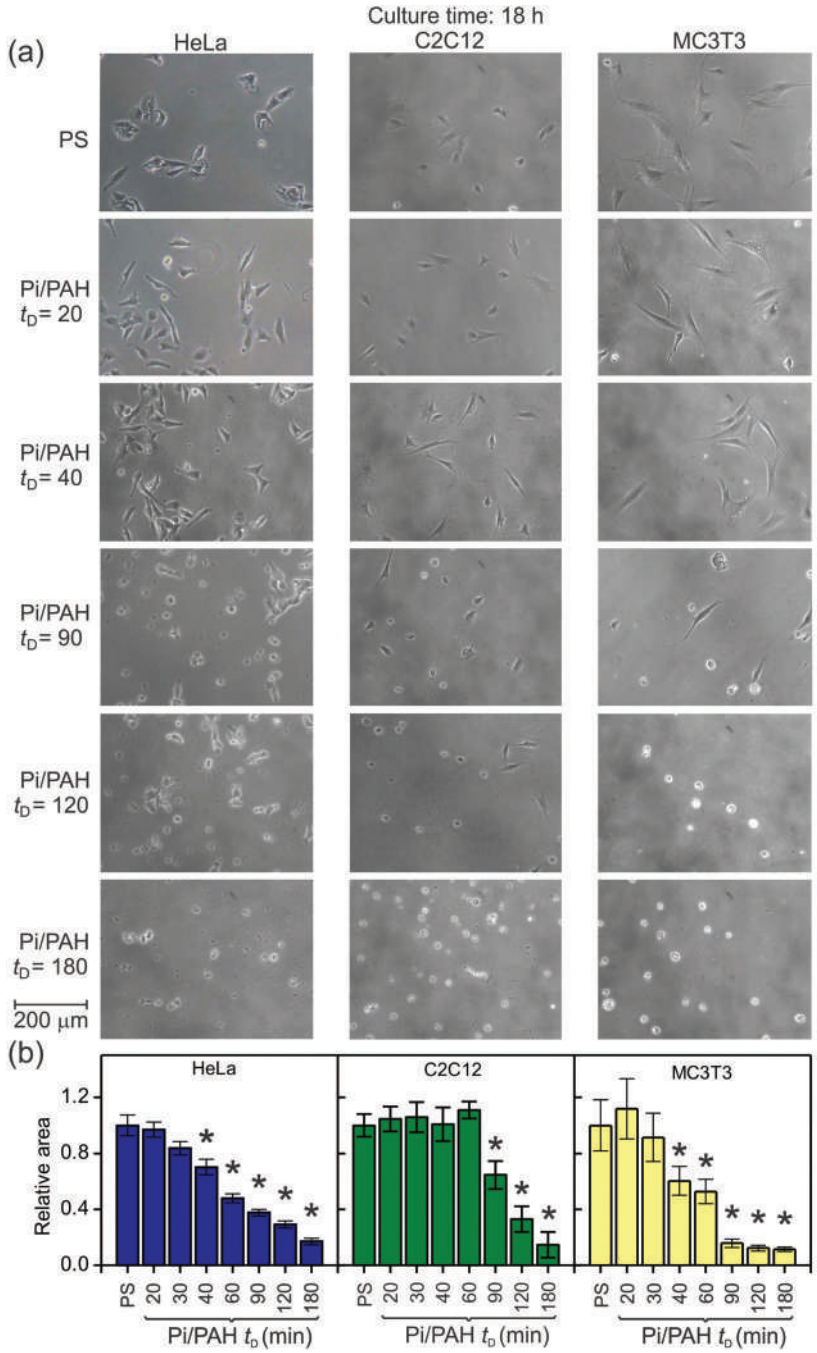

Fig. 1 Cell adhesion characteristics for PS and Pi/PAH-coated PS substrates with different deposition times, t_D (in min), as indicated in the figure. Typical contrast phase microimages (a) and histograms of relative average spreading areas (b) of HeLa, C2C12 and MC3T3 cells 18 h post-seeding on PS, and Pi/PAH-coated PS with different t_D. One mL of supplemented medium containing 20 000 cells was poured onto each coated substrate. More than 50 cells were considered for each condition, and the standard errors are included. Asterisks indicate significant differences with respect to PS after performing ANOVA and Fischer test with p = 0.05. In the histograms, the average cell spreading area evaluated from Pi/PAH-coated substrates with t_D = 30 and 60 min is also shown. A cell type-dependent behavior is observed; the relative spreading area decreases rather monotonously from a certain t_D. For t_D = 180 min an antiadherent coating is obtained irrespective of the cell line.

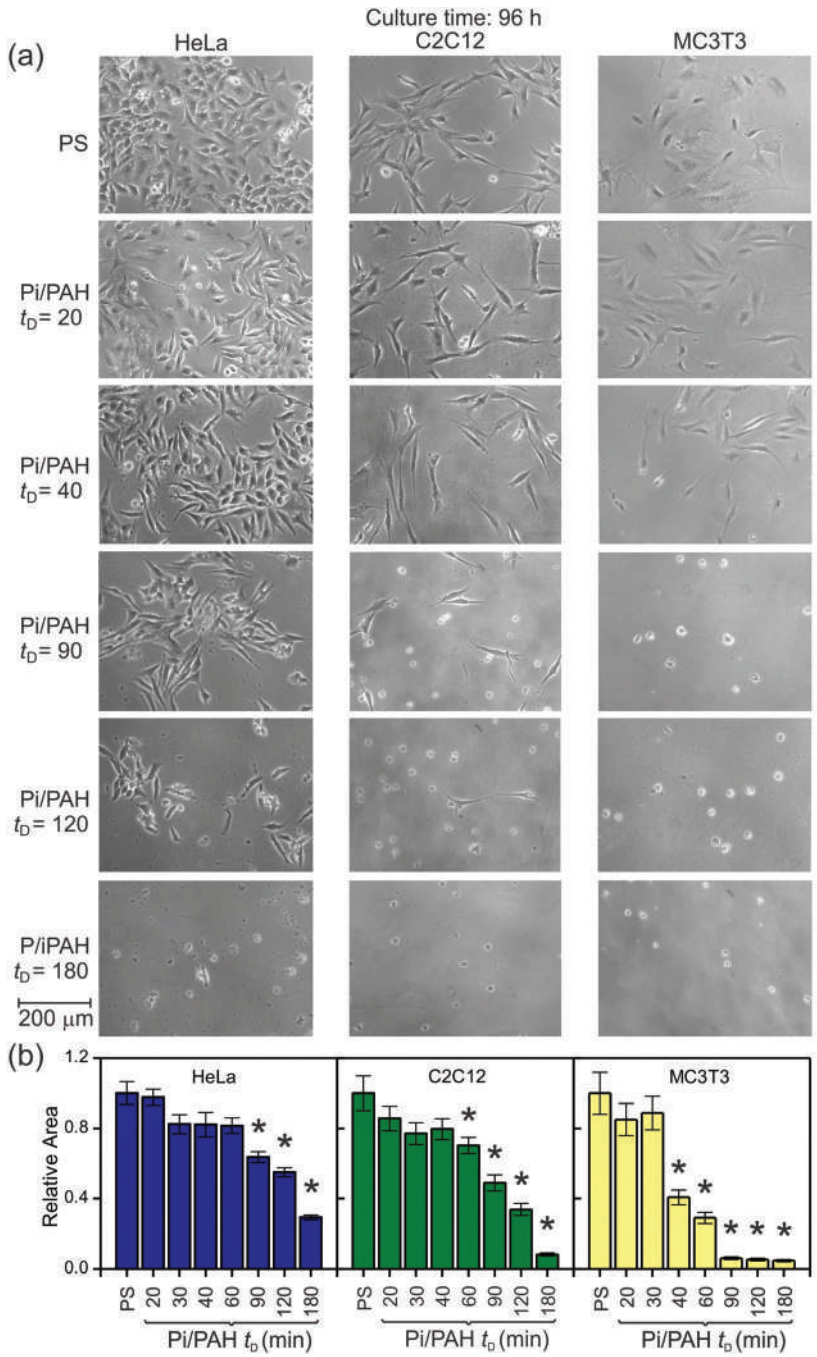

Fig. 2 Cell adhesion characteristics of HeLa, C2C12 and MC3T3 cells 96 h post-seeding on PS and Pi/PAH-coated PS substrates with different deposition times, t_D (in min), as indicated in the figure. Typical contrast phase microimages (a) and histograms of relative average spreading areas (b). Seeding condition are the same as for adhesion experiments 18 h post-seeding. Supplemented medium (1 mL) containing 20 000 cells was poured onto each coated substrates. Histograms also include the average cell spreading area evaluated from Pi/PAH-coated substrate with t_D = 30 and 60 min. More than 50 cells were considered for the analysis at each condition, and the standard errors are included. Asterisks indicate significant differences with respect to PS after performing ANOVA and Fischer test with p = 0.05. Cell adhesion decreases with increasing t_D, this tendency being more remarkable for MC-3T3 cell line as a relatively poor adhesion from t_D = 40 min and only small rounded cells for 90 < t_D < 180 min, can be distinguished. For all cell lines antiadherent surfaces are obtained for t_D = 180 min.

75, 102, 110 and 123 nm, respectively, can be estimated from Fig. S1.†

From phase contrast photographs taken every day for 1–4 days, the cell spreading area was measured. The same results were obtained from samples on both PS and glass coverslips irrespective of the cell line.

Cell average spreading areas from cultures inspected 18 h post-seeding (Fig. 1) indicate that cell adhesion characteristics

exhibit a cell type-dependent behavior. For HeLa and C2C12 cell lines, even for t_D = 120 min, it is possible to find cells adhered to the film surface, but for MC3T3 cells, adherence is very poor. Pi/PAH-coated substrates, with t_D = 180 min, exhibit almost antiadhesive properties for all cell lines tested. Histograms (Fig. 1b) represent the relative average cell spreading areas referred to that obtained for control PS or glass and add further details related to the cell type-dependent adhesion. For coatings with t_D up to 30 min HeLa and MC3T3 cell lines exhibit adhesion characteristics similar to those for PS or glass. For HeLa cells 18 h post-seeding, the average relative spreading area decreases continuously from a value close to 1 for Pi/PAH-coated substrates with t_D = 20 min to 0.15 ± 0.04 for Pi/PAH-coated substrates with t_D = 180 min. For HeLa cells the average spreading area on PS is 960 ± 40 μm^2. For MC3T3 cells, 2250 ± 120 μm^2 in average spreading area, the behavior is similar to that obtained from HeLa cells, although cell adhesion characteristics are poorer, particularly for $t_D \geq$ 90 min. C2C12 cells on Pi/PAH-coated substrates with $t_D <$ 90 min present a similar behaviour to that of cells adhered to PS or glass. For larger values of t_D, a monotonous decrease in the spreading area is observed. Histograms of C2C12 cells, with 1500 ± 100 μm^2 in average spreading area, show that the relative spreading area for Pi/PAH-coated substrates with t_D up to 60 min is similar to that obtained on glass or PS. Then, the average relative spreading area decreases monotonously to about 0.12 for Pi/PAH-coated substrates with t_D = 180 min.

Cell adhesion experiments carried out 96 h after seeding (Fig. 2) show a change in the cell type-dependent behavior. The adhesion of HeLa cells to Pi/PAH-coated substrates improves irrespective of t_D. In contrast, a slight decrease is observed for C2C12 cells for most t_D and a more pronounced decrease in MC3T3 cell adhesion to Pi/PAH-coated substrates with t_D > 40 min. These cells exhibit the worst adhesion characteristics for substrates with larger t_D. Furthermore, C2C12 cells appear to adhere better than MC3T3 cells, but remain poorer than HeLa cells (Fig. 2).

Similarly to the observed behavior in 18 h post-seeding adhesion experiments, no adhered cells can be observed 96 h after seeding onto Pi/PAH coating with t_D = 180 min, irrespective of the cell line. Histograms of cell relative average spreading areas measured 96 h post-seeding indicate that the HeLa cell relative average spreading area remains approximately above 0.8 up to t_D = 60 min and decreases to 0.6 for t_D = 90 and 120 min, exhibiting a better behavior than C2C12 cells, which in turn present relative areas below 0.5 for t_D = 90 and 120 min. The decrease in the relative cell spreading area shown in the histograms, particularly for MC-3T3 cells and t_D > 40 min, should be attributed to the increase in the number of rounded cells coming from anoikis, cell death induced by poor adhesion to the substrate, and to the increase in the reference cell area from cells on control PS. The latter consideration is also applicable to C2C12 cells.

To get further insight into cell adhesion, we measured the average propagation area of the cell adhering to PS and the Pi/PAH-coated substrate with t_D = 40 min (60 ± 7 nm thickness) at short times, *i.e.*, t < 20 h post-seeding to quantify the cytoplasm expansion evolution (Fig. S2 in the ESI†). Data indicate that MC3T3 and C2C12 cells adhere faster to PS than HeLa cells. Furthermore, cell adhesion to Pi/PAH-coated PS exhibits a similar behavior to that of PS substrate, but with slower adhesion kinetics. This fact appears to be consistent with the improved HeLa cell adhesion observed 96 h after seeding in comparison with adhesion 18 h post-seeding.

The data indicate that Pi/PAH-coated substrates exhibit good adhesion properties for all cell lines evaluated, provided t_D is shorter than a certain value (*ca.* 40 min) and the coating thickness is close to 60 ± 7 nm, thus cells appear to sense the rigid substrate underneath. For longer t_D, the deposited

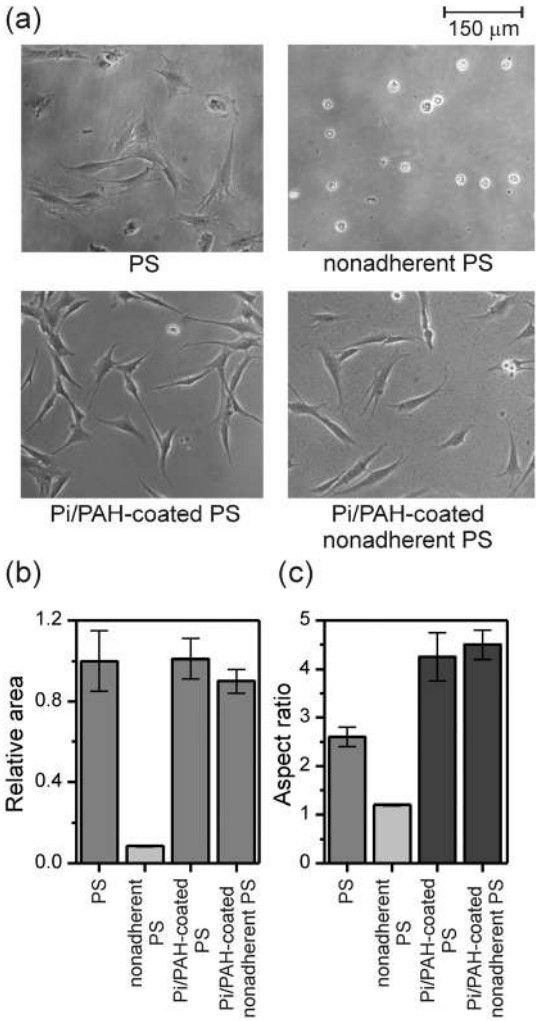

Fig. 3 C2C12 cell adhesion characteristics 24 h post-seeding on PS, nonadherent PS, Pi/PAH-coated PS and Pi/PAH-coated nonadherent PS substrates with t_D = 20 min. (a) Typical contrast phase microimages. Scale bar is included. (b) Relative average cell spreading area. (c) Cell aspect ratio. Standard errors are included, and ANOVA analysis with Fisher test with significant differences (p = 0.05) is shown in gray scale. More than 50 cells were considered for the analysis. The Pi/PAH coating with t_D = 20 min (25 ± 2 nm thick) turns a nonadherent substrate into an adhesive one.

(Pi/PAH) mass and the coating thickness increase and cells cannot properly feel the rigid substrate underneath, exhibiting a cell type-dependent behavior.

In agreement with the above observations, enhanced adhesion for HeLa, C2C12 and MC3T3 cells is obtained by Pi/PAH coating for t_D = 20 min (25 ± 2 nm coating thickness) of bacteriological PS, the latter exhibiting scarce adhesion to eukaryote cells. The adhesion characteristics of C2C12 cells adhered to PS, bacteriological nonadherent PS and Pi/PAH-coated PS and Pi/PAH-coated nonadherent PS are depicted in Fig. 3. Relative average cell spreading areas show a significant increase according to ANOVA analysis with Fisher test (p = 0.05) for cells on Pi/PAH-coated nonadherent PS in comparison to nonadherent PS. Additionally, the aspect ratio is larger for cells on Pi/PAH-coated substrates than for cells on either PS or nonadherent PS.

3.2. Enhanced cell adhesion of thermally annealed Pi/PAH coatings

In the previous section the cell adhesion characteristics of three cell lines seeded on PS and Pi/PAH-coated substrates were described. In general, an acceptable adhesion was obtained for all cell lines tested for coated substrates with t_D up to 40 min, and a coating thickness of 60 ± 7 nm. For larger

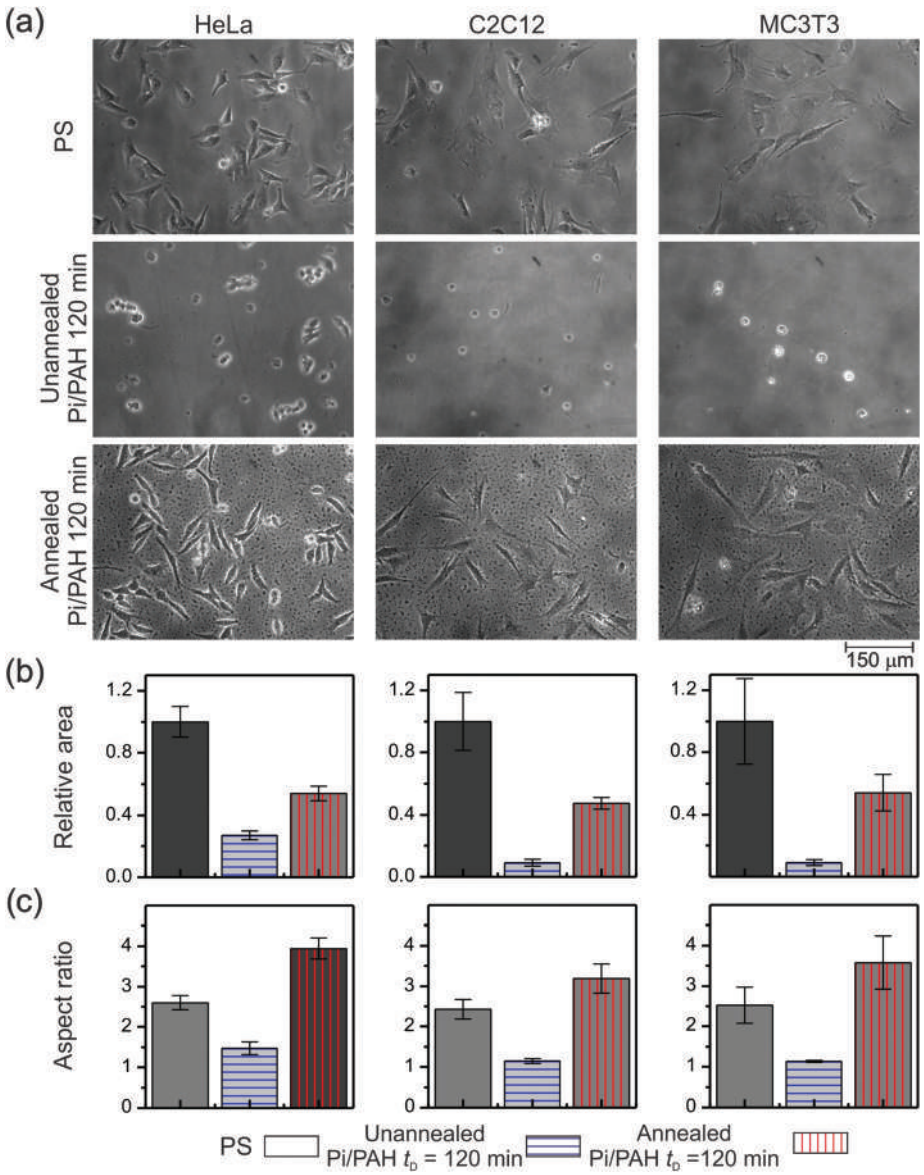

Fig. 4 Cell adhesion modulation by thermal annealing of Pi/PAH-coated substrates. Typical contrast phase microimages (a), relative average cell spreading area (b) and aspect ratio (c) of HeLa, C2C12 and MC3T3 cells, 36 h post-seeding on PS, and annealed and unannealed Pi/PAH-covered PS with t_D = 120 min, as indicated in the figure. The annealing of air dried Pi/PAH antiadherent Pi/PAH-coated substrates with t_D = 120 min renders a surface with acceptable cell adhesion properties; cell aspect ratio plots indicate that cells on annealed substrates are more tapered than on control PS.

t_D, cell adhesion became progressively worse. For t_D = 120 min, the coating thickness reaches 110 ± 10 nm, and almost no adhesion was observed. In this section a strategy to improve cell adhesion to Pi/PAH-coated substrates with t_D = 120 min, is presented.

In previous works we have recently reported that the cell adhesion properties of polyelectrolyte multilayers can be tuned by thermal annealing,[37,43,44] and that a gradient of physicochemical properties to obtain a local control of the cell adhesion characteristics can be set by applying a thermal gradient along a polyelectrolyte multilayer.[45] With this notion in mind, the modulation of the cell-adhesion properties of Pi/PAH-coated substrates *via* thermal annealing was studied. To this end, air dried Pi/PAH-coated substrates with t_D = 120 min were annealed for 3 day at 37 °C in the cell culture incubator, and then UV-sterilized and seeded with HeLa, C2C12 and MC3T3 cells in the appropriate supplemented medium.

Cell adhesion to Pi/PAH-coated substrates with t_D = 120 min increases significantly after annealing (Fig. 4). This effect is observed even for preosteoblast MC3T3 cells that exhibited no adhesion at all to unannealed films with the same t_D. From the optical images (Fig. 4), it is also possible to distinguish changes in the appearance of the Pi/PAH film after the annealing process. Furthermore, it is worth noting, that cells on annealed Pi/PAH-coated substrates are more tapered in shape than on control PS or glass, and MC3T3 and C2C12 cells have more and longer filopodia. These observations are in agreement with histograms of the relative average cell spreading area and cell aspect ratio (Fig. 4b and c). The former approaches a value close to 0.6, and the aspect ratio becomes significantly larger than that obtained from cells on PS.

3.3. Immunostaining

Fluorescence images of the cell cytoskeleton, focal adhesions and cell nucleus were obtained by staining F-actin, vinculin protein and by counterstaining with DAPI (Fig. 5 and 6). Cell adhesion to a substrate involves the linkage between the cytoskeleton and the extracellular matrix and this connection is mediated by specialized dynamic multiprotein structures that evolve from adhesion sites, at the early stages of the adhesion process, to mature focal adhesions coupled to actin filaments. During this process, actin filaments are also assembled into stress fibers, affecting cell structure and polarity. Vinculin, a cytosolic focal adhesion protein recruited during the assembly of early adhesion sites, is postulated to act as a mechanosensor. The head domain of vinculin protein interacts with talin and integrins and the tail domain transmits force *via* linking to the actin cytoskeleton.[46]

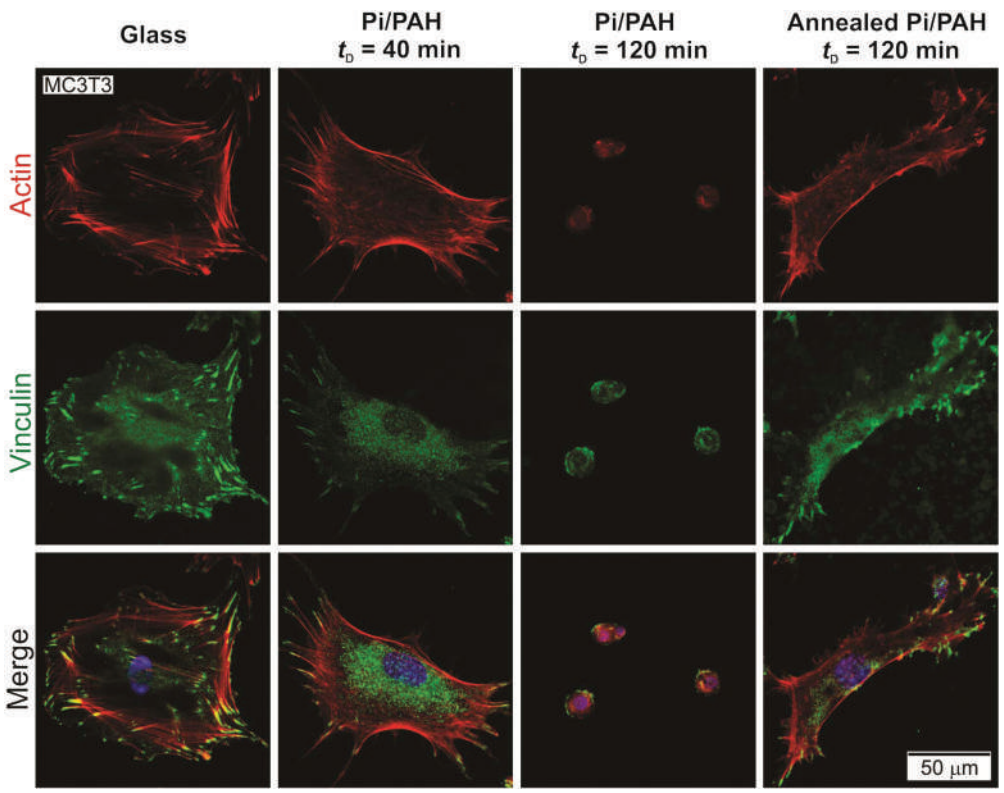

Fig. 5 Fluorescence microimages of MC3T3 preosteoblast cells stained for actin (red), vinculin (green) and nuclei (blue). The staining was done 24 h after cell seeding on glass and Pi/PAH-coated substrates, as indicated in the figure. Mature focal adhesions can be seen in cells on glass and Pi/PAH-coated substrates with t_D = 40 min, although for the latter, the cell spreading area is slightly smaller and a more stellate shape is observed. For Pi/PAH-coated substrates with t_D = 120 min, cell adhesion is very poor and cells are rounded. After annealing, cell adhesion significantly improves and well-defined focal adhesions and a more tapered morphology can be distinguished.

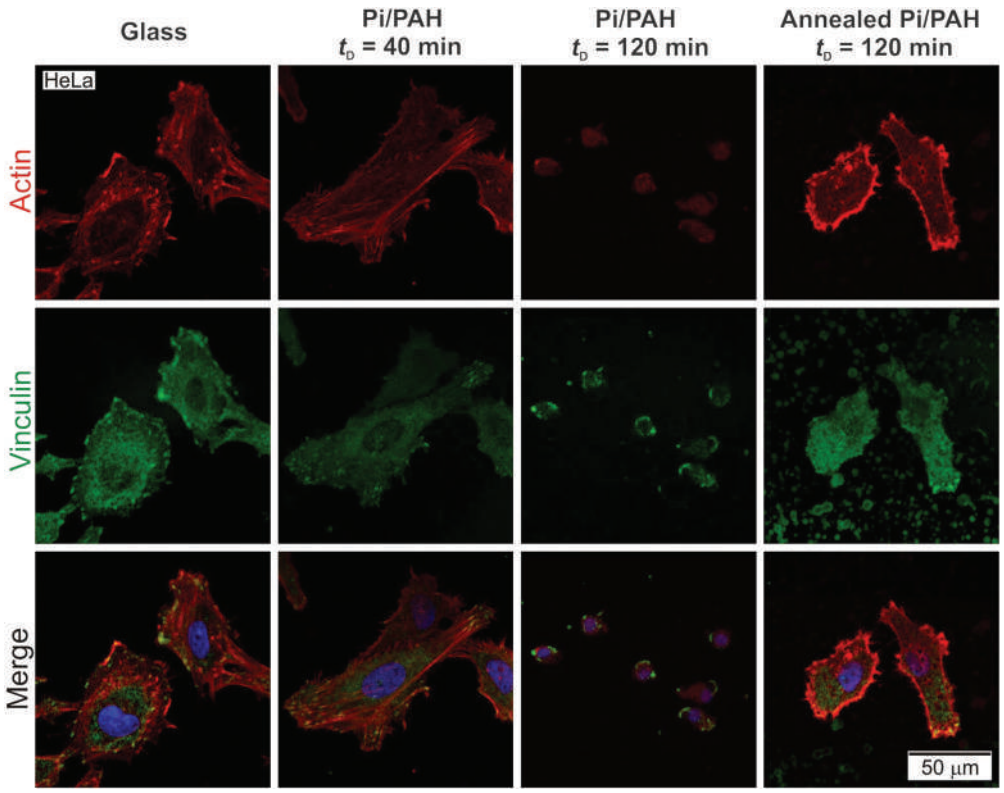

Fig. 6 Fluorescence microimages of HeLa cells stained for actin (red), vinculin (green) and nuclei (blue). The staining was made 24 h after cell seeding on glass and Pi/PAH-coated substrates as indicated in the figure. Focal adhesions can be seen in cells on glass as well as on Pi/PAH-coated substrates with t_D = 40 min; there are small differences between both as regards HeLa cells. For Pi/PAH-coated substrates with t_D = 120 min, cell adhesion is very poor and cells are rounded. For annealed Pi/PAH-coated substrates with t_D = 120 min, the cell spreading area increases but remains smaller than for glass.

For glass substrates, extended cells with actin filaments connecting adhesion contacts can be distinguished in HeLa and MC3T3 cells. Focal adhesions appear as green spots oriented in the direction of the cytoplasm protrusion, particularly visible at the cell edges. Focal adhesions are larger for MC3T3 cells than for HeLa cells.

MC3T3 cells seeded on Pi/PAH-coated substrates with t_D = 40 min (60 ± 7 nm thick) exhibit a slightly smaller cell spreading area and a larger number of filopodia than for cells on glass (Fig. 5). MC3T3 cells on Pi/PAH-coated substrates with t_D = 40 min are more stellate and the size of focal adhesions becomes smaller than for cells adhered to glass. On Pi/PAH-coated substrates with t_D = 120 min, MC3T3 cells show poor cytoskeleton spreading, a few focal adhesions and a diffuse fluorescence image. After annealing the cell spreading area increases but remains smaller than for glass or Pi/PAH-coated substrates with t_D = 40 min, and some well-developed focal adhesions connected to actin filaments can be observed at protrusions of the tapered cytoskeleton.

From HeLa cell staining experiments (Fig. 6), a similar description to that given for MC3T3 is applicable. In this case, similarly to MC3T3 cells, upon annealing Pi/PAH-coated substrates with t_D = 120 min HeLa cell adhesion improves significantly but it is worse than that observed on glass.

3.4. Viability assay (MTT)

Cell viability for all cell lines employed in this work was evaluated by measuring the absorbance of the formazan product metabolized by viable cells adhered to PS, unannealed Pi/PAH-coated PS with t_D = 40 min, and annealed Pi/PAH-coated substrate with t_D = 120 min (Fig. 7). Unannealed Pi/PAH-coated substrates with t_D = 40 min were used instead of t_D = 120 min because no adhesion is observed for the latter. For HeLa and C2C12 cells, viability was evaluated at 24, 48, 72 and 96 h after seeding, and for MC3T3 cells at 24, 72, 96 and 168 h post-seeding, as the duplication time of this osteoblastic cell line is longer than for the others.

Provided that cell metabolism remains unaltered for the different substrates, the absorbance is proportional to the number of cells, which increases approaching a quasi-exponential relationship with t, irrespective of the cell line (Fig. 7). As expected, HeLa and C2C12 cells show larger proliferation rates as compared to preosteoblasts. Results indicate a larger proliferation for the annealed Pi/PAH-coated substrate with t_D = 120 min than for the unannealed Pi/PAH-coated substrate with t_D = 40 min, irrespective of the cell line. For the control, unannealed and annealed Pi/PAH coated-substrates, the number of cells increases with t following a quasi-exponential

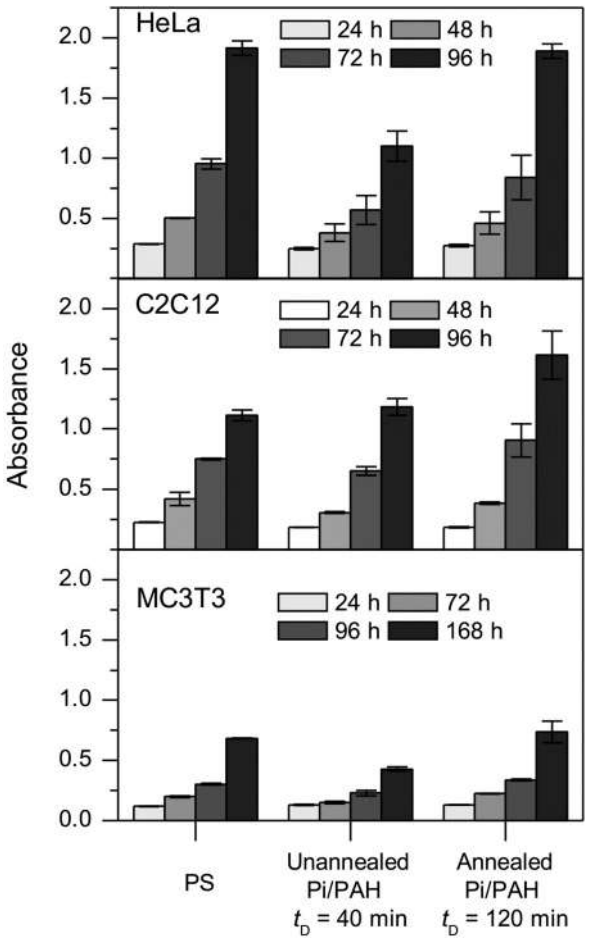

Fig. 7 Cell proliferation of HeLa, C2C12 and MC3T3 cells on PS, unannealed Pi/PAH-coated PS with t_D = 40 min and annealed Pi/PAH-coated PS with t_D = 120 min, measured by MTT. Formazan absorbance was measured after culturing on the control and Pi/PAH-coated substrates for times indicated (hours) in the figure. Standard errors are included. For HeLa and C2C12 cell lines the viability assay was performed at 24, 48, 72 and 96 h, while for MC-3T3 preosteoblast cell line, due to its longer duplication time, absorbance measurements were performed at 24, 72, 96 and 168 h. In all the substrates a quasi-exponential relationship between absorbance and time is observed. Thus, Pi/PAH-coated substrates thin enough to allow cell adhesion as well as annealed substrates exhibit acceptable cell proliferation.

relationship. Moreover, in the case of C2C12 cells, proliferation appears to be larger for the annealed Pi/PAH coated substrate than for control PS. In the previous section, it was shown that C2C12 average adhesion areas measured 18 h post-seeding on Pi/PAH-coated substrates with $20 \leq t_D \leq 60$ min are similar to that observed for PS (Fig. 1), a behavior not observed for the other cell lines. Thus, the effect of the Pi/PAH coating on cell adhesion and viability is particularly enhanced for this cell line, at least within the time frame studied in this work.

To probe the long-term viability of cells cultured on Pi/PAH-coated substrates, we cultured MC3T3 cells for 20 days, obtaining a confluent monolayer (see Fig. S3 in the ESI†) of viable cells tested by the Trypan Blue exclusion test.

3.5. Topographic features, mechanical properties, wettability and protein adsorption

The growth kinetics of Pi/PAH coatings followed by quartz crystal microbalance with dissipation and surface plasmon resonance spectroscopy, for different concentrations of PAH in the range $0.025 < c_{PAH} < 0.2$ mg mL^{-1} was reported in a previous work.[25] The chemistry of the synthesized films was studied by X-ray photoelectron spectroscopy and Fourier transform infrared spectroscopy, and it was demonstrated that protonated amine groups interact electrostatically with orthophosphate ions and that hydrogen bondings also play a key role.

Atomic force microscopy has been proven to be a valuable technique to study the topographical and mechanical properties of nanofilms.[47] In order to understand the physical cues involved in the modulation of cell adhesion to the multifunctional coatings presented herein, we then evaluated the film topography and stiffness, and the effect of the thermal annealing on these properties.

AFM imaging of Pi/PAH-coatings allowed following the surface topography changes upon increasing the deposition time t_D (Fig. 8). For short t_D and coating thickness of about 60 ± 7 nm, Pi/PAH supramolecular networks assembled and deposited on PS or glass substrates exhibited a rather heterogeneous surface coating with mounds and valleys 0.2–1 μm long and with height differences on the order of 10 nm, as can be seen from the cross-section profile and height distribution. In this case, the roughness resulted in 3.1 ± 0.5 nm. For an intermediate t_D and coating thickness of 90 ± 8 nm, the topography of the films was found to be more homogeneous, exhibiting a narrowed height distribution with a standard deviation below 5 nm and a roughness of 2.2 ± 0.4 nm. Conversely to this intermediate smoother surface, a further increase in t_D to 120 min, and a concomitant increase of the coating thickness to 110 ± 10 nm, led to the recovery of a coarse surface with protrusions 0.2–0.9 μm in length and a height deviation above 10 nm, and a roughness close to 3 nm. AFM results indicated that the change in roughness was too small to induce the variations in the cell adhesion characteristics with the t_D reported previously.

On the other hand, nanomechanical AFM characterization did not reveal a significant difference between the elastic modulus (E) of the Pi/PAH coatings for t_D of 40 min and 120 min (Fig. 9), which was on the order of 200 kPa as obtained by the Sneddon's contact mechanics model, assuming a parabolic tip and a plane surface contact (see Methods for further details). We should bear in mind that in these experiments, AFM nanoindentation is on the order of 30 nm to reliably measure the material elasticity avoiding a substrate contribution, a quantity smaller than the coating thickness. However, cells are shown to sense rigid structures below soft coatings about 1 μm thick.[10,48] Thus, cells are thoroughly able to sense the rigid substrate under the Pi/PAH coating, and the substrate influence possibly increases provided that t_D is short. When the deposited mass is high enough, the coating thickness increases and adhesion characteristics become worse,

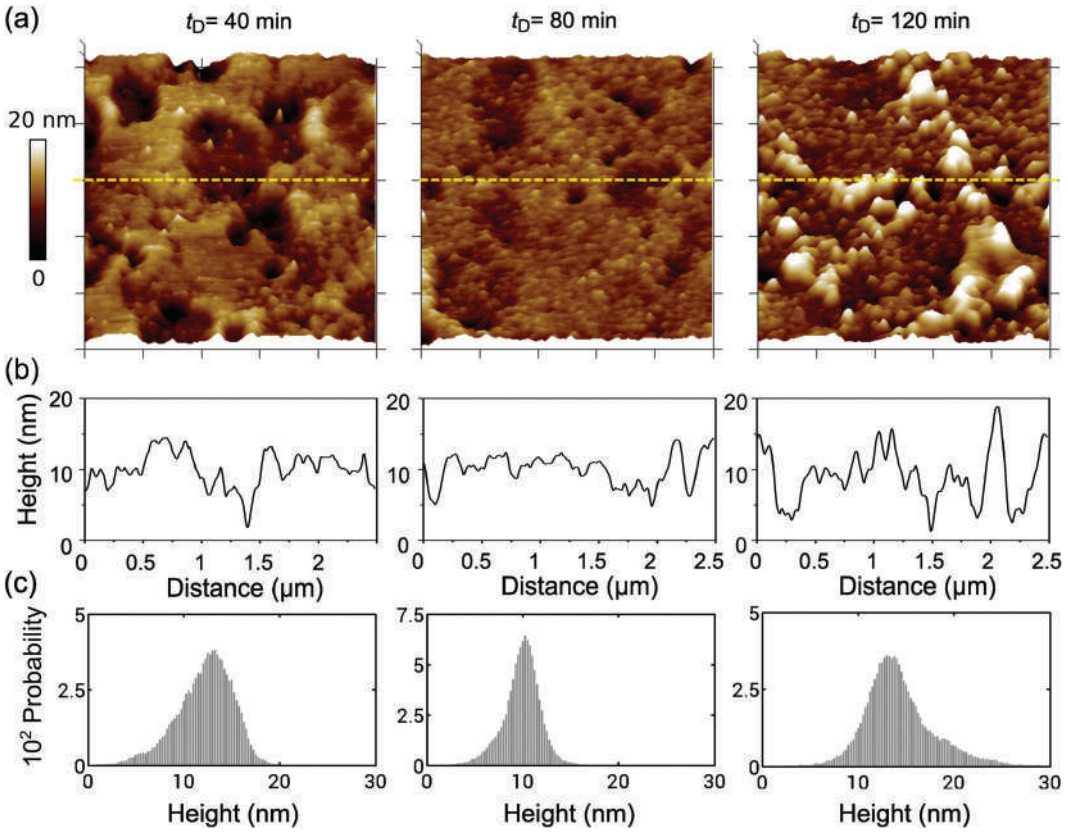

Fig. 8 Topographic characteristics of Pi/PAH-coated substrates with t_D = 40 min, t_D = 80 min, and t_D = 120 min. (a) Tapping mode 2.5 × 2.5 μm^2 *in situ* AFM images. (b) Typical profiles and (c) height histograms from images depicted in (a) are included for each t_D. The zero height value was taken as the minimum height value for each image. For Pi/PAH-coated substrates with t_D = 120 min, the histogram shows a shift of the height towards larger values, which is coherent with larger protrusions as seen in (a).

which is in agreement with the poor mechanical properties of the Pi/PAH film and a decrease in the rigid substrate influence. In any case, it is worth noting that two cooperative effects could contribute to the observed change in cell adhesion: the intrinsic poor mechanical properties of Pi/PAH networks and the change in the morphological characteristics of the Pi/PAH complex aggregates, although for t_D < 120 min roughness changes seem to be small.

Cell adhesion modulation has been previously achieved by depositing a compliant soft polymer layer upon a stiff support of controlled topography to obtain different thicknesses of the coating.[49] Stiff materials can be sensed through soft ones, depending on the thickness of the coating and the magnitude of its deformation.[50–53] Cells on a relatively soft coating adhered to an underlying stiff substrate sense a complex stiffness,[8,48,50] that is, the result of the combination of the stiffness of both the upper soft material and the rigid substrate underneath. This strategy of cell adhesion modulation by changing the substrate stiffness that cells are able to sense avoids chemical changes that are present in other strategies such as chemical cross-linking, the incorporation of particles to strengthen the coating, and changes in the assembling conditions (ionic strength, pH, *etc.*). Furthermore, this strategy, based on complex stiffness, has been successfully applied to enhance the adhesion characteristics of endothelial cells with respect to smooth muscle cells,[10] and to generate a gradient in mechanical properties to direct fibroblast motility.[41] The material proposed in our work is suitable for the strategy described above.

In a similar vein, we characterized the influence of the thermal annealing on the nanomechanical and topological properties of the Pi/PAH coatings (Fig. 9 and 10) as well as on wettability, surface charge and the adsorption of proteins (Fig. 10).

Remarkably, Pi/PAH-coated films with t_D = 120 min became stiffer after thermal annealing with a 2.5-fold increase in their elastic modulus (Fig. 9). Furthermore, the topography of the films changed considerably to a structured surface (Fig. 10a and b), with micron-sized topographic features hundreds of nm in height. The smaller protrusions in the unannealed coating became coalesced micron-sized features, resembling a ripening process driven by the decrease in surface energy.[54] This grainy, rugged appearance was previously evidenced on the optical images of the annealed Pi/PAH-coated substrates (see Fig. 4 and 10). The Young's modulus histogram was consistent with a single distribution, independent of the structured nature of the annealed film. In fact, AFM force measurements from different places of the film revealed the same

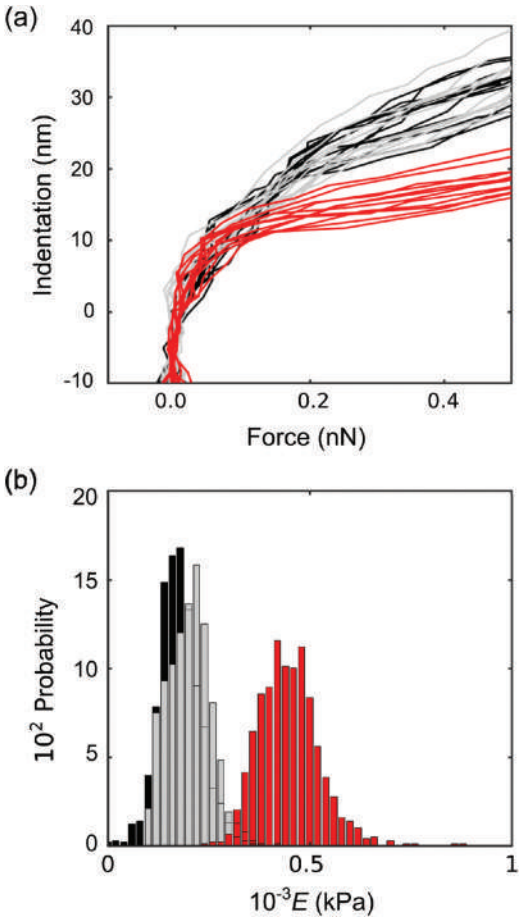

Fig. 9 Pi/PAH coating stiffness measured by AFM nanoindentation. (a) Typical indentation *vs.* force curves for unannealed coatings with t_D = 40 min (gray), t_D = 120 min (black), and for annealed coatings with t_D = 120 min (red). (b) Young's modulus distributions of the same films, which yield elasticity values of 178 ± 51 kPa, and 201 ± 52 kPa for unannealed coatings with 40 min and 120 min of t_D respectively, and 449 ± 74 kPa for annealed coatings with 120 min of t_D.

indentation characteristics for protrusions and valleys, and consequently similar stiffness values (Fig. 9). This indicates that after annealing Pi/PAH complexes become stiffer at both protrusions and valleys. It is worth noting that Pi/PAH Young's modulus changes upon annealing within the range of values in which the cell adhesion characteristics of a large number of cell lines are significantly affected, as has been reported.[55–57]

AFM measurements of coatings, either unannealed or annealed, immersed in PBS and left in the cell culture incubator up to 4 days, exhibit similar characteristics to samples freshly prepared and eventually thermally treated but without aging in PBS (Fig. S4 in the ESI†). Thus, Pi/PAH-coated substrates appear to remain stable along the experiments with cells.

Upon annealing the contact angle increased from 39.7° ± 0.9° for unannealed coatings to 65° ± 2° after annealing (Fig. 10c). Thus, the hydrophobicity increases. Intermediate contact angle values of around 90° would favor cell adhesion,[12] although recently it has been reported that the water contact angle is not a good predictor of biological responses to materials.[58]

The ζ-potential was determined for unannealed and annealed Pi/PAH-coated substrates by measuring the electroosmotic flow employing a dip cell device. Results indicate a decrease in the negative surface charge; the ζ-potential was −37 ± 5 mV and −8 ± 6 mV for unannealed and annealed substrates, respectively (Fig. 10d). If we consider that, in most of cases, charged/polar surfaces are highly wettable surfaces, then it is plausible to observe a decrease in hydrophilicity upon decreasing the surface charge.

Furthermore, FN protein adsorption on the unannealed coated substrate with either t_D = 40 min or t_D = 120 min as well as on annealed substrates with t_D = 120 min, was evaluated by QCM-D experiments (Fig. 10e). These experiments were carried out to get more information about the effect of thermal annealing on the behavior of the coating with cells in the medium. Pi/PAH coatings were deposited on the QCM crystals outside the chamber and reinserted into the chamber, either freshly prepared or after annealing. Firstly, samples were rinsed with HEPES buffer solution until frequency stabilization, then 20 mg mL^{-1} FN solution in buffer was injected and the adsorbed mass evaluated, after rinsing again with buffer. The adsorption of FN produces a frequency decrease of $-\Delta f$ = 98 ± 2, $-\Delta f$ = 109 ± 2, and $-\Delta f$ = 93 ± 2 Hz, for unannealed Pi/PAH-coatings with either t_D = 40 min or t_D = 120 min and annealed Pi/PAH coating with t_D = 120 min, respectively. These figures were obtained from QCM-D curves shown in Fig. S5 of the ESI;† dissipation indicates that proteins adsorb forming a rather compact layer, and the Sauerbrey equation is applicable.

Not only the amount but the conformation[12] of adsorbed adherent protein is important for cell adhesion. Cells adhere to a substrate *via* interaction with proteins from the serum. BSA is present at high concentration in the serum containing culture media, and adsorbs first in a nonspecific manner conferring antiadherent properties, but adherent proteins displace BSA in substrates exhibiting good cell adhesion. Recently evidence has been reported from a well-characterized polyelectrolyte multilayer (PEM) assembled with poly(4-styrenesulfonic acid) (PSS) and poly(diallyl-dimethylammonium chloride) (PDADMAC) demonstrating the dynamic nature of the interface interacting with cells and the importance of the strength of the interaction of proteins with the substrate.[59] For cells to sense the rigidity of the substrate, they need to attach to adhesion proteins that are adsorbed on the interface with a sufficiently high interaction energy; cells cannot "feel" what they cannot hold. The authors showed an abrupt change in cell adhesion with a small change in the PEM thickness by varying the number of deposited layers but maintaining its roughness constant. Thus, the stiffness of the substrate was not an important property in the observed adhesion behavior. Furthermore, the authors studied the competition of proteins from the culture medium with preadsorbed labeled BSA on PEMs with variable surface charge. In fact, several factors

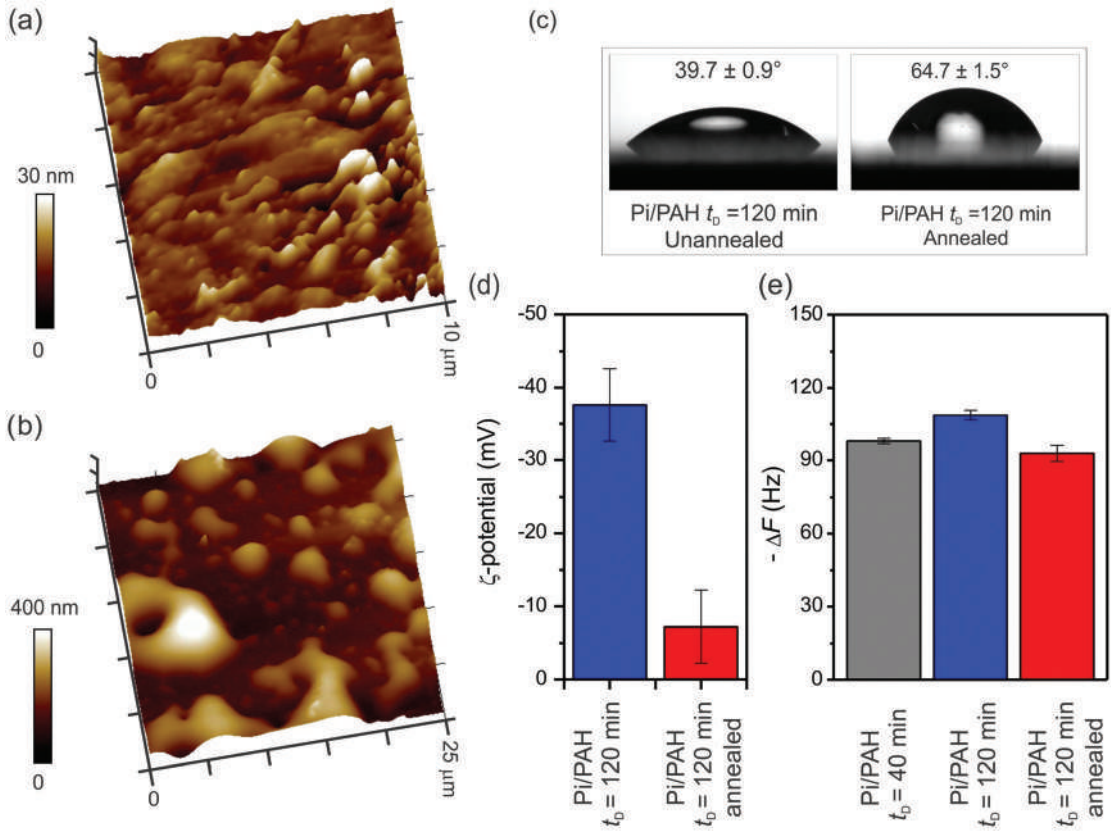

Fig. 10 AFM peak force height images for unannealed (a) and annealed (b) Pi/PAH-coated substrates with t_D = 120 min. Scales are indicated in each image. A dramatic change in the substrate roughness is produced after annealing. Contact angle measurements (c), surface potential values (d) and decrease in frequency after fibronectin adsorption (e) are also depicted. A decrease in the surface charge and the hidrophilicity of the substrates after annealing is inferred. There is a small change in the fibronectin adsorbed mass for the tested substrates.

affect protein adsorption, namely, topographic features,[60] stiffness,[7] surface charge and type of exposed functional groups[62] and interface water content and structure.[61]

Our FN adsorption experiments indicate that the amount of adsorbed FN is similar for the different Pi/PAH-coated substrates, the maximum relative difference is about 10%. The adsorption of FN tends to increase in going from a Pi/PAH-coated substrate with t_D = 40 min to a Pi/PAH-coated substrate with t_D = 120 min, and then to decrease slightly after the thermal annealing of the latter. Furthermore, the negative ζ-potential decreases under annealing from about −40 mV to −10 mV, and the surface becomes more hydrophobic, as indicated by contact angle measurements. Protein adsorption is expected to be larger on charged surfaces than on neutral ones, due to interactions with protein positive patches.[59] Assuming an average increase in $-\Delta F \approx 100$ Hz, the calculated mass of adsorbed FN, ≈354 ng cm^{-2}, is on the order of that reported by other authors,[62] who found good adhesion for HUVEC cells to self-assembled monolayers with preadsorbed FN providing tripeptide sequence Arg–Gly–Asp (RGD) based adhesion sites.[62] Moreover, by varying the thickness of Pi/PAH coating from 25 nm to about 100 nm we observed a gradual decrease in cell adhesion rather than an abrupt change (Fig. 1 and 2). The staining of actin and vinculin shows a change in the size of focal adhesions and stress fibers (Fig. 5 and 6), diminishing in going from coatings with about 60 nm to 110 nm for t_D = 120 min. After annealing cell adhesion and the expression of vinculin significantly increase. These results suggest that after annealing, cell adhesion improves significantly due to a combined effect of the increase in the coating hydrophobicity, stiffness, and a dramatic change in the coating morphology. With these facts in mind, the effect of thermal annealing is further analyzed.

It has been proposed that the thermal annealing of polyelectrolyte multilayers (PEMs) enhances the interaction of oppositely charged polyelectrolytes by increasing polyelectrolyte chain motility,[44] rendering a more compact film. In the case of Pi/PAH system, complexes are formed in solution with the Pi anion easily interacting electrostatically with the protonated amine moieties from PAH, and then deposited onto the substrate. Thus, following the thermal treatment employed in this work, only low charge redistribution would be expected. It has also been reported that the relative humidity affects the stiffness and thickness of polymeric films with an internal structure rich in hydrogen-bonding sites.[63] It is a well-documented fact that cell adhesion is enhanced in substrates with

increased contact angle[12] and augmented stiffness,[56] the latter affecting the cell colony organization in a cell type-dependent manner.[64] More recently, the effect of polymer hydration/dehydration on cell interactions with its environment, either *in vitro* or *in vivo*, has been reviewed,[65] and it has been pointed out that hydration at the interface influences cell adhesion, proliferation, motility and differentiation. Furthermore, the water state depends on the architecture of hydrated polymer chain playing a key role in protein function.[66–68] Cells interact with coatings through adsorbed proteins from biological fluids. These proteins adsorb on the surface in a certain amount and conformation that is affected by the substrate stiffness.[59,61,69–71] Thus, surface hydration and stiffness should affect cell phenotype through a complex mechanism. According to the presented data, the thermal annealing increases the stiffness of the coating and improves cell adhesion only when the annealing is performed in the cell culture incubator without immersion in PBS. Thus, a partial irreversible dehydratation appears to occur and would not only contribute to the coating stiffness but to the change in its topography and the cooperative modulation of the protein adsorption process. These facts appear to be reflected in the cell adhesion characteristics. The topographic changes in the Pi/PAH coatings would be associated with a redistribution of material that could also affect the complex stiffness sensed by adhered cells.

4. Conclusions

Cell adhesion modulation for three different cell lines, HeLa epithelial cells, C2C12 murine myoblasts, and MC3T3 murine preosteoblasts, in a biomimetic single step fabricated Pi/PAH-based coating is presented. This material offers good biocompatibility with an augmented proliferation in the case of C2C12 cell line.

Cell adhesion characteristics were modified following two strategies: (i) the mass of the coating films is controlled by the deposition time of the Pi/PAH complex and a cell type-dependent behavior is observed with the film mass; (ii) the Pi/PAH-coated substrate with t_D = 120 min is annealed by thermal treatment at 37 °C. Cell adhesion for all cell lines tested improved significantly after annealing.

The adhesion kinetics evaluated at short times exhibited the same behavior for Pi/PAH-coated substrate as for PS or glass control substrates, although with a smaller rate in the former case.

Wettability determinations, topographic data and rigidity measurements indicate that the stiffness of the coating plays a key role in cell adhesion modulation. For Pi/PAH-coated films with low t_D, the underlying glass or PS substrate is sensed by cells through a complex stiffness mechanism. On the other hand, for longer t_D the thermal annealing improves the adhesion characteristics imparting enhanced rigidity to the film material, mainly due to dehydration, increasing the hydrophobicity, the stiffness, and drastically changing the morphology of the coatings. These changes upon annealing are reflected in the differences of cell morphological parameters evaluated from cells adhered to unannealed and annealed Pi/PAH coatings in comparison with control substrates.

In summary, the proposed biomimetic material coating is biocompatible and suitable to modulate cell adhesion by simple experimental protocols. This material may be used either to improve cell adhesion or as an antifouling surface. The former would be achieved employing thin coatings or annealed ones, and antifouling properties would be obtained for thicker unannealed coatings. Thus, it becomes a promising material for biological applications, making a profitable use of the multifunctional capabilities of this supramolecular assembly.

Conflicts of interest

There are no conflicts to declare.

Acknowledgements

This work was supported by the Consejo Nacional de Investigaciones Científicas y Técnicas (CONICET, Argentina) (Grant No. PIP 0602), Agencia Nacional de Promoción Científica y Tecnológica (ANPCyT, Argentina; PICT-2010-2554, and PICT-2013-0905), the Austrian Institute of Technology GmbH (AIT–CONICET Partner Group: "Exploratory Research for Advanced Technologies in Supramolecular Materials Science", Exp. 4947/11, Res. No. 3911, 28-12-2011), and Universidad Nacional de La Plata (UNLP). M. A. P., W. A. M., C. vB., M. L. C., L. I. P. and O. A. are staff members of CONICET.

Notes and references

1 C. Monge, J. Almodóvar, T. Boudou and C. Picart, Spatio-Temporal Control of LbL Films for Biomedical Applications: From 2D to 3D, *Adv. Healthcare Mater.*, 2015, **4**, 811, DOI: 10.1002/adhm.201400715.

2 N. P. Murphy and K. J. Lampe, Mimicking Biological Phenomena in Hydrogel-based Biomaterials to Promote Dynamic Cellular Responses, *J. Mater. Chem. B*, 2015, **3**, 7867, DOI: 10.1039/C5TB01045D.

3 B. M. Sciari, R. Londono and S. F. Badylak, Strategies for Skeletal Muscle Tissue Engineering: Seed vs. Soil, *J. Mater. Chem. B*, 2015, **3**, 7881, DOI: 10.1039/C5TB01045D.

4 L. Bačáková, E. Filová, F. Rypáček, V. Švorčík and V. Starý, Cell Adhesion on Artificial Materials for Tissue Engineering, *Phys. Res.*, 2004, **53**, S35.

5 D. F. Williams, Biocompatibility Pathways: Biomaterials-Induced Stimuli Inflammation, Mechanotrasduction, and Principles of Biocompatibility Control, *ACS Biomater. Sci. Eng.*, 2017, **3**, 2, DOI: 10.1021/acsbiomaterials.6b00607.B.

6 J. D. Mih, A. Marinkovic, F. Liu, A. S. Sharif and D. J. Tschumperlin, Matrix stiffness reverses the effect of actomyosin tension on cell proliferation, *J. Cell Sci.*, 2015, **125**, 5974, DOI: 10.1242/jcs.108886.

7 C. Rianna and M. Radmacher, Influence of Microenvironment Topography and Stiffness on the Mechanics and Motility of Normal and Cancer Renal Cells, *Nanoscale*, 2017, **9**, 11222, DOI: 10.1039/C7NR02940C.

8 A. Buxboim, I. L. Ivanovska and D. E. Discher, Matrix Elasticity, Cytoskeletal Forces and Physics of the Nucleus: How Deeply do Cells 'Feel' Outside and in?, *J. Cell Sci.*, 2010, **123**, 297, DOI: 10.1242/jcs.041186.

9 M. J. Paszek, N. Zahir, K. R. Johnson, J. N. Lakins, G. I. Rozenberg, A. Gefen, C. A. Reinhart-King, S. S. Margulies, M. Dembo, D. Boettiger, D. A. Hammer and V. M. Weaver, Tensional Homeostasis and the Malignant Phenotype, *Cancer Cell*, 2005, **8**, 241, DOI: 10.1016/j.ccr.2005.08.010.

10 H. Chang, H. Zhang, M. Hu, X.-Ch. Chen, K.-F. Ren, J.-L. Wanga and J. Ji, Surface Modulation of Complex Stiffness via layer-by-layer Assembly as a Facile Strategy for Selective Cell Adhesion, *Biomater. Sci.*, 2015, **3**, 352, DOI: 10.1039/C4BM00321G.

11 S. Mehrotra, S. C. Hunley, K. M. Pawelec, L. Zhang, I. Lee, S. Baek and C. Chan, Cell Adhesive Behavior on Thin Polyelectrolyte Multilayers: Cells Attempt to Achieve Homeostasis of Its Adhesion Energy, *Langmuir*, 2010, **26**, 12794, DOI: 10.1021/la101689z.

12 L. Bačáková, E. Filová, M. Parizek, T. Ruml and V. Švorčík, Modulation of cell adhesion, proliferation and differentiation on materials designed for body implants, *Biotechnol. Adv.*, 2011, **29**, 739, DOI: 10.1016/j.biotechadv.2011.06.004.

13 K. Anselme, L. Ploux and A. Ponche, Cell/Material Interfaces: Influence of Surface Chemistry and Surface Topography on Cell Adhesion, *J. Adhes. Sci. Technol.*, 2010, **24**, 831, DOI: 10.1163/016942409X12598231568186.

14 A. Engler, L. Bačáková, C. Newman, A. Hategan, M. Griffin and D. Discher, Substrate Compliance Versus Ligand Density in Cell on Gel Responses, *Biophys. J.*, 2004, **86**, 617, DOI: 10.1016/S0006-3495(04)74140-5.

15 P. M. Kharkar, K. L. Kiick and A. M. Kloxin, Designing Degradable Hydrogels for Orthogonal Control of Cell Microenvironments, *Chem. Soc. Rev.*, 2013, **42**, 7335, DOI: 10.1039/c3cs60040h.

16 Sh. Saxena, M. W. Spears Jr., H. Yoshida, J. C. Gaulding, A. J. García and A. Lyon, Microgel Film Dynamics Modulate Cell Adhesion Behavior, *Soft Matter*, 2014, **10**, 1356, DOI: 10.1039/C3SM52518J.

17 *Manipulation of Nanoscale Materials: An Introduction to Nanoarchitectonics*, ed. K. Ariga, Royal Society of Chemistry, Cambridge, 2012. DOI: 10.1039/9781849735124.

18 H. Wang, D.-W. Zhang and Z.-T. Li, in *Hydrogen Bonded Supramolecular Materials, Lectures in Chemistry*, ed. Z.-T. Li and L.-Z. Wu, Springer-Verlag, Berlin Heidelberg, 2015, p. 185. DOI: 10.1007/978-3-662-45780-1_6.

19 J. Simon and P. Bassoul, *Design of Molecular Materials: Supramolecular Engineering*, John Wiley & Sons, Chichester, 2000. ISBN 0-471-97371-8.

20 Q. Ye, F. Zhou and W. Liu, Bioinspired Catecholic Chemistry for Surface Modification, *Chem. Soc. Rev.*, 2011, **40**, 4244, DOI: 10.1039/C1CS15026J.

21 J. Sedó, J. Saiz-Poseu, F. Busqué and D. Ruiz-Molina, *Adv. Mater.*, 2013, **25**, 653, DOI: 10.1002/adma.201202343.

22 B. P. Lee, P. B. Messersmith, J. N. Israelachvili and J. H. Waite, *Annu. Rev. Mater. Res.*, 2011, **41**, 99, DOI: 10.1146/annurev-matsci-062910-100429.

23 Y. Liu, K. Ai and L. Lu, Polydopamine and Its Derivative Materials: Synthesis and Promising Applications in Energy, Environmental, and Biomedical Fields, *Chem. Rev.*, 2014, **114**, 5057, DOI: 10.1021/cr400407a.

24 L. Han, X. Lu, K. Liu, K. Wang, L. Fang, L.-T. Weng, H. Zhang, Y. Tang, F. Ren, C. Zhao, G. Sun, R. Liang and Z. Li, Mussel-Inspired Adhesive and Tough Hydrogel Based Nanoclay Confined Dopamine Polymerization, *ACS Nano*, 2017, **11**, 2561, DOI: 10.1021/acsnano.6b05318.

25 W. A. Marmisollé, J. Irigoyen, D. Gregurec, S. Moya and O. Azzaroni, Supramolecular Surface Chemistry: Substrate-Independent, Phosphate-Driven Growth of Polyamine-Based Multifunctional Thin Films, *Adv. Funct. Mater.*, 2015, **25**, 4144, DOI: 10.1002/adfm.201501140.

26 L. D'Agostino and A. Di Luccia, Polyamines Interact with DNA as Molecular Aggregates, *Eur. J. Biochem.*, 2002, **269**, 4317, DOI: 10.1046/j.1432-1033.2002.03128.x.

27 L. D'Agostino, M. di Pietro and A. Di Luccia, Nuclear Aggregates of Polyamines are Supramolecular Structures that Play a Crucial Role in Genomic DNA Protection and Conformation, *FEBS J.*, 2005, **272**, 3777, DOI: 10.1111/j.1742-4658.2005.04782.x.

28 N. Kröger, R. Deutzman, C. Bergsdorf and M. Sumper, Species-specific Polyamines from Diatoms Control Silica Morphology, *Proc. Natl. Acad. Sci. U. S. A.*, 2000, **97**, 14133, DOI: 10.1073/pnas.260496497.

29 S. R. Cicco, D. Vona, R. Gristina, E. Sardella, R. Ragni, M. Lo Presti and G. M. Farinola, Biosilica from Living Diatoms: Investigations on Biocompatibility of Bare and Chemically Modified Thalassiosira weissflogii Silica Shells, *Bioengineering*, 2016, **3**, 35, DOI: 10.3390/bioengineering3040035.

30 K. Lutz, C. Gröger, M. Sumper and E. Brunner, Biomimetic Silica Formation: Analysis of the Phosphate-induced Self-assembly of Polyamines, *Phys. Chem. Chem. Phys.*, 2005, **7**, 2812, DOI: 10.1039/B505945C.

31 M. Sumper and N. Kröger, Silica Formation in Diatoms: the Function of Long-chain Polyamines and Silaffins, *J. Mater. Chem.*, 2004, **14**, 2059, DOI: 10.1039/B401028K.

32 E. Brunner, K. Lutz and M. Sumper, Biomimetic Synthesis of Silica Nanospheres Depends on the Aggregation and Phase Separation of Polyamines in Aqueous Solution, *Phys. Chem. Chem. Phys.*, 2004, **6**, 854, DOI: 10.1039/B313261G.

33 Y. Huang, P. G. Lawrence and Y. Lapitsky, Self-Assembly of Stiff, Adhesive and Self-Healing Gels from Common

Polyelectrolytes, *Langmuir*, 2014, **30**, 7771, DOI: 10.1021/la404606y.

34 P. G. Lawrence and Y. Lapitsky, Ionically Cross-linked Poly(allylamine) as a Stimulus-Responsive Underwater Adhesive: Ionic Strength and pH Effects, *Langmuir*, 2015, **31**, 1564, DOI: 10.1021/la504611x.

35 Y. Zhang, M. Herling and D. M. Chenoweth, General Solution for Stabilizing Triple Helical Collagen, *J. Am. Chem. Soc.*, 2016, **138**, 9751, DOI: 10.1021/jacs.6b03823.

36 R. Lakra, M. S. Kiran, R. Usha, R. Mohan, R. Sundaresan and P. S. Korrapati, Enhanced Stabilization of Collagen by Furfural, *Int. J. Biol. Macromol.*, 2014, **65**, 252, DOI: 10.1016/j.ijbiomac.2014.01.040.

37 N. E. Muzzio, D. Gregurec, E. Diamanti, J. Irigoyen, M. A. Pasquale, O. Azzaroni and S. E. Moya, Cell Adhesion: Thermal Annealing of Polyelectrolyte Multilayers: An Effective Approach for the Enhancement of Cell Adhesion, *Adv. Mater. Interfaces*, 2017, **4**, 1600126, DOI: 10.1002/admi.201770007.

38 J. Hutter and J. Bechhoefer, Calibration of Atomic Force Microscope Tips, *Rev. Sci. Instrum.*, 1993, **64**, 1868, DOI: 10.1063/1.1143970.

39 D. C. Lin, E. K. Dimitriadis and F. Horkay, Robust Strategies for Automated AFM Force Curve Analysis—II: Adhesion-Influenced Indentation of Soft, Elastic Materials, *J. Biomech. Eng.*, 2007, **129**, 430, DOI: 10.1115/1.2720924.

40 S. A. Chizhik, Z. Huang, V. V. Gorbunov, N. K. Myshkin and V. V. Tsukruk, Micromechanical Properties of Elastic Polymeric Materials as Probed by Scanning Force Microscopy, *Langmuir*, 1998, **14**, 2606, DOI: 10.1021/la980042p.

41 H. Shulha, A. Kovalev, N. Myshkin and V. V. Tsukruk, Some Aspects of AFM Nanomechanical Probing of Surface Polymer Films, *Eur. Polym. J.*, 2004, **40**, 949, DOI: 10.1016/j.eurpolymj.2004.01.021.

42 J. C. W. Corbett, F. McNeil-Watson, R. O. Jack and M. Howarth, Measuring Surface zeta Potential Using Phase Analysis Light Scattering in a Simple Dip Cell Arrangement, *Colloids Surf., A*, 2012, **396**, 169, DOI: 10.1016/j.coldufa.2011.12.065.

43 E. Diamanti, N. E. Muzzio, D. Gregurec, J. Irigoyen, M. A. Pasquale, O. Azzaroni, M. Brinkmann and S. E. Moya, Impact of Thermal Annealing on Wettability and Antifouling Characteristics of Alginate Poly-l-Lysine Polyelectrolyte Multilayer Films, *Colloids Surf., B*, 2017, **145**, 328, DOI: 10.1016/j.colsurfb.2016.05.013.

44 N. E. Muzzio, M. A. Pasquale, E. Diamanti, D. Gregurec, M. Martinez Moro, O. Azzaroni and S. E. Moya, Enhanced Antiadhesive Properties of Chitosan/Hyaluronic Acid Polyelectrolyte Multilayers Driven by Thermal Annealing: Low Adherence for Mammalian Cells and Selective Decrease in Adhesion for Gram-positive Bacteria, *Mater. Sci. Eng., C*, 2017, **80**, 677, DOI: 10.1016/j.msec.2017.07.016.

45 N. E. Muzzio, M. A. Pasquale, S. E. Moya and O. Azzaroni, Tailored Polyelectrolyte Thin Film Multilayers to Modulate Cell Adhesion, *Biointerphases*, 2017, **12**, 04E403, DOI: 10.1116/1.5000588.

46 S. Di Cio and J. E. Gautrot, Cell Sensing of Physical Properties at the Nanoscale: Mechanisms and control of Cell Adhesion and Phenotype, *Acta Biomater.*, 2016, **30**, 26, DOI: 10.1016/j.actbio.2015.11.027.

47 V. V. Tsukruk and S. Singamaneni, *Scanning Probe Microscopy of Soft Matter: Fundamentals and Practices*, Wiley-VCH Verlag & Co. KGaA, Weinheim, Germany, 2012.

48 S. Shimomura, H. Matsuno and K. Tanaka, Effect of Mechanical Instability of Polymer Scaffolds on Cell Adhesion, *Langmuir*, 2013, **29**, 11087, DOI: 10.1021/la4027706.

49 C.-H. R. Kuo, J. Xian, J. D. Brenton, K. Franze and E. Sivaniah, Complex Stiffness Gradient Substrates for Studying Mechanotactic Cell Migration, *Adv. Mater.*, 2012, **24**, 6059, DOI: 10.1002/adma.201202520.

50 J. M. Maloney, E. B. Walton, C. M. Bruce and K. J. Van Vliet, Influence of Finite Thickness and Stiffness on Cellular Adhesion-induced Deformation of Compliant Substrata, *Phys. Rev. E: Stat. Phys., Plasmas, Fluids, Relat. Interdiscip. Top.*, 2008, **78**, 041923, DOI: 10.1103/PhysRevE.78.041923.

51 S. Sen, A. J. Engler and D. E. Discher, Matrix Strains Induced by Cells: Computing How Far Cells can Feel, *Cell. Mol. Bioeng.*, 2009, **2**, 39, DOI: 10.1007/s12195-009-0052-z.

52 A. Buxboim, K. Rajagopal, A. E. Brown and D. E. Discher, How Deeply Cells Feel: Methods for Thin Gels, *J. Phys.: Condens. Matter*, 2010, **22**, 194116, DOI: 10.1088/0953-8984/22/19/194116.

53 W. T. Chen, Computation of Stresses and Displacements in a Layered Elastic Medium, *Int. J. Eng. Sci.*, 1971, **9**, 775, DOI: 10.1016/0020-7225(71)90072-3.

54 A. Kabalnov, Ostwald Ripening and Related Phenomena, *J. Dispersion Sci. Technol.*, 2001, **22**, 1, DOI: 10.1081/DIS-100102675.

55 J. Solon, I. Levental, K. Sengupta, P. C. Georges and P. A. Janmey, Fibroblast Adaptation and Stiffness Matching to Soft Elastic Substrates, *Biophys. J.*, 2007, **93**, 4453, DOI: 10.1529/biophysj.106.101386.

56 S. Y. Tee, J. Fu, C. S. Chen and P. A. Janmey, Cell Shape and Substrate Rigidity Both Regulate Cell Stiffness, *Biophys. J.*, 2011, **100**, L25, DOI: 10.1016/j.bpj.2010.12.3744.

57 A. Schneider, G. Francius, R. Obeid, P. Schwinté, J. Hemmerlé, B. Frisch, P. Schaaf, J.-C. Voegel, B. Senger and C. Picart, Polyelectrolyte Multilayers with a Tunable Young's Modulus: Influence of Film Stiffness on Cell Adhesion, *Langmuir*, 2006, **22**, 1193, DOI: 10.1021/la0521802.

58 M. R. Alexander and P. Williams, Water Contact Angle is not a Good Predictor of Biological Responses to Materials, *Biointerphases*, 2017, **12**, 026201, DOI: 10.1116/1.4989843.

59 C. J. Arias, R. L. Surmaitis and J. B. Schelenoff, Cell Adhesion and Proliferation on the "Living" Surface of a Polyelectrolyte Multilayer, *Langmuir*, 2016, **32**, 5412, DOI: 10.1021/acs.langmuir.6b00784.

60 M. S. Lord, M. Foss and F. Basenbacher, Influence of Nanoscale Surface Topography on Protein Adsorption and Cellular Response, *Nano Today*, 2010, **5**, 66, DOI: 10.1016/j.nantod.2010.01.001.

61 S. Kakinoki, J. H. Seo, Y. Inoue, K. Ishihara, N. Yui and T. A. Yamaoka, A Large Mobility of Hydrophilic Molecules at the Outmost Layer Controls the Protein Adsorption and Adhering Behavior with the Actin Fiber Orientation of Human Umbilical Vein Endothelial Cells (HUVEC), *J. Biomater. Sci., Polym. Ed.*, 2013, **24**, 1320, DOI: 10.1080/09205063.2012.757726.

62 Y. Arima and H. Iwata, Preferential Adsorption of Cell Adhesive Proteins from Complex media on self-assembled monolayers and its effect on Subsequent Cell Adhesion, *Acta Biomater.*, 2015, **26**, 72, DOI: 10.1016/j.actbio.2015.08.033.

63 A. J. Nolte, N. D. Treat, R. E. Cohen and M. E. Rubner, Effect of Relative Humidity on the Young's modulus of Polyelectrolyte Multilayer Films and Related Nonionic Polymers, *Macromolecules*, 2008, **41**, 5793, DOI: 10.1021/ma800732j.

64 M. K. Shah, I. H. García-Pak and E. M. Darling, Influence of Inherent Mechanophenotype on Competitive Cellular Adherence, *Ann. Biomed. Eng.*, 2017, **45**, 2036, DOI: 10.1007/s10439-017-1841-5.

65 G. Kerch, Polymer Hydration and Stiffness at Biointerfaces and Related Cellular Processes, *Nanomedicine*, 2018, **14**, 13, DOI: 10.1016/j.nano.2017.08.012.

66 M. Grossutti and J. R. Dutcher, Correlation Between Chain Architecture and Hydration Water Structure in Polysaccharides, *Biomacromolecules*, 2016, **17**, 1198, DOI: 10.1021/acs.biomac.6b00026.

67 M. Grossutti, E. Bergmann, B. Baylis and J. R. Dutcher, Equilibrium Swelling, Interstitial Forces, and Water Structuring in Phytoglycogen Nanoparticle Films, *Langmuir*, 2017, **33**, 2810, DOI: 10.1021/acs.langmuir.7b00025.

68 P. Ball, Water as an Active Constituent in Cell Biology, *Chem. Rev.*, 2008, **108**, 74, DOI: 10.1021/cr068037a.

69 M. Antia, G. Baneyx, K. E. Kubow and V. Vogel, Fibronectin in Aging Extracellular Matrix Fibrils is Progressively Unfolded by Cells and Elicits an Enhanced Rigidity Response, *Faraday Discuss.*, 2008, **139**, 229. PMCID: PMC2613444.

70 J. H. Seo, K. Sakai and N. Yui, Adsorption State of Fibronectin on Poly(dimethylsiloxane) Surfaces with Varied Stiffness can Dominate Adhesion Density of Fibroblasts, *Acta Biomater.*, 2013, **9**, 5493, DOI: 10.1016/j.actbio.2012.10.015.

71 M. M. Ouberai, K. Xu and M. E. Welland, Effect of the Interplay Between Protein and Surface on the Properties of Adsorbed Protein Layers, *Biomaterials*, 2014, **35**, 6157, DOI: 10.1016/j.biomaterials.2014.04.012.